Chinese Journal of Natural Medicines

**Micranthin B alleviates metabolic dysfunction–associated steatohepatitis by targeting G3BP1 to improve stress granule–mediated endoplasmic reticulum stress**

Yang Cheng, Jingyi Wang, Mengmeng He, Enyi Wu, Shengtao Ye, Ying Zheng, Yanqiu Zhang, Lingyi Kong, Hao Zhang

**Citation:** Yang Cheng, Jingyi Wang, Mengmeng He, Enyi Wu, Shengtao Ye, Ying Zheng, Yanqiu Zhang, Lingyi Kong, Hao Zhang, Micranthin B alleviates metabolic dysfunction–associated steatohepatitis by targeting G3BP1 to improve stress granule–mediated endoplasmic reticulum stress, Chinese Journal of Natural Medicines, 2026, 24(6), 757–768. doi: 10.1016/S1875–5364(26)61189–2.

View online: https://doi.org/10.1016/S1875–5364(26)61189–2

Chinese Journal of Natural Medicines 24 (2026) 757-768

Contents lists available at ScienceDirect

Chinese Journal of Natural Medicines

journal homepage: www.cjnmcpu.com/

Original article

# Micranthin B alleviates metabolic dysfunction-associated steatohepatitis by targeting G3BP1 to improve stress granule-mediated endoplasmic reticulum stress

Yang Cheng, Jingyi Wang, Mengmeng He, Enyi Wu, Shengtao Ye, Ying Zheng, Yanqiu Zhang*, Lingyi Kong*, Hao Zhang*

*State Key Laboratory of Natural Medicines, Joint International Research Laboratory of Target Discovery and New Drug Innovation (Ministry of Education), Affiliated Jiangning Hospital of Chinese Medicine, China Pharmaceutical University, Nanjing 210009, China*

ARTICLE INFO

*Article history:*
Received 23 October 2025
Revised 12 January 2026
Accepted 24 January 2026
Available online 20 June 2026

*Keywords:*
MASH
Micranthin B
G3BP1
Stress granule
Endoplasmic reticulum homeostasis

ABSTRACT

Ras-GTPase activating protein SH3 domain-binding protein 1 (G3BP1), a core component of stress granules (SGs), is highly expressed in several liver diseases. SG assembly has also been observed in metabolic disorders, suggesting that this process may be a promising therapeutic target. Using a high-content drug screening approach based on G3BP1 expression, we identified Micranthin B (MB), a diterpenoid from *Isodon lophanthoides* (Buch.-Ham. ex D. Don) Hara, as a compound that alleviates metabolic dysfunction-associated steatohepatitis (MASH) by targeting G3BP1 and inhibiting SG formation. MB administration significantly alleviated MASH progression in both high-fat, high-cholesterol (HFHC) diet-induced mouse model and palmitic acid (PA)-stimulated hepatocytes. Mechanistically, MB inhibited histone deacetylase 6 (HDAC6)-mediated deacetylation of G3BP1, thereby suppressing SG formation. This prevented SG-mediated recruitment of the N-glycosylation-related proteins SEC61 translocon subunit beta (SEC61B) and calnexin (CANX), reduced the accumulation of misfolded or unfolded proteins, and alleviated endoplasmic reticulum (ER) stress. These findings suggest that MB has therapeutic potential in the treatment of MASH.

## 1. Introduction

Metabolic dysfunction-associated steatotic liver disease (MASLD) is a major cause of liver disease globally, with an estimated prevalence of approximately 32.4% [1, 2]. Metabolic dysfunction-associated steatohepatitis (MASH) is a more severe form of MASLD and is characterized by steatosis affecting more than 5% of hepatocytes, lobular inflammation, hepatocyte ballooning, and, in some cases, fibrosis [3, 4]. Patients with MASH have a substantially increased risk of liver cirrhosis and MASLD-associated hepatocellular carcinoma (MASLD-HCC) [3]. A previous study projected that, by 2025, MASH would surpass viral hepatitis as the leading indication for liver transplantation [5]. Although Resmetirom has been approved by the United States Food and Drug Administration (FDA) as the first drug for the treatment of MASH, current treatment options remain insufficient. There is therefore an urgent need to identify new anti-MASH therapies.

Endoplasmic reticulum (ER) stress is a prominent feature of MASH progression [6]. Hepatic lipid accumulation induces ER stress and activates the unfolded protein response (UPR), which contributes to steatosis [7, 8]. UPR activation promotes lipogenesis, insulin resistance (IR), and hepatocyte injury [8]. If ER stress is not resolved, it can eventually lead to hepatocyte death [8]. N-linked glycosylation is essential for glycoprotein quality control and protein folding in the ER. It also plays an important role in ER stress activation and UPR induction [9]. Plasma protein N-linked glycosylation has been extensively studied in liver disease and may serve as a biomarker for MASLD and other hepatic disorders [10]. In the ER, N-linked glycosylation begins with the synthesis of lipid-linked oligosaccharides (LLOs) by various N-glycosylation processing enzymes (ALGs). The oligosaccharyltransferase (OST) complex then transfers the oligosaccharide chain to the polypeptide backbone [11]. The OST complex also anchors the glycosylation chain to the SEC61 translocon and glycosylates peptide chains as they enter through this channel [12]. This step is critical for protein modification by N-glycosylation [13]. Additionally, calnexin (CANX) and calreticulin (CALR), together with the disulfide isomerase ERp57, mediate quality control during N-glycosylation and promote proper folding of newly synthesized glycoproteins [14, 15]. When misfolded or non-native proteins accumulate excessively in the ER, ER stress is triggered. Mild ER stress activates the UPR and helps restore ER homeostasis. In contrast, excessive or prolonged ER stress causes persistent UPR activation, which leads to lipid metabolic disorders, inflammatory factor release, and hepatocyte apoptosis, thereby promoting MASH progression [16]. Despite its importance, the role of N-glycosylation in MASH remains unclear.

Ras-GTPase activating protein SH3 domain-binding protein 1 (G3BP1) is a core structural component and molecular switch of stress granules (SGs) and is mainly localized in the cytoplasm.

* Corresponding author.
*E-mail addresses:* yqzhang1610@126.com (Y. Zhang); cpu_lykong@126.com (L. Kong); zhanghao@cpu.edu.cn (H. Zhang)

https://doi.org/10.1016/S1875-5364(26)61189-2

G3BP1 has been extensively studied in hepatocellular carcinoma (HCC), where it promotes tumor proliferation, metastasis, and invasion through multiple oncogenic pathways [17]. Both G3BP1 mRNA and protein levels are significantly increased in HCC tissues compared with adjacent non-tumorous liver tissues, and high G3BP1 expression is strongly associated with poor prognosis, indicating G3BP1 as important prognostic biomarker [18]. In our study, G3BP1 was also markedly upregulated in MASH cell and animal models. As a central node in SG ribonucleoprotein networks, G3BP1 regulates SG assembly and disassembly [19, 20]. Previous studies have found that in pancreatic β-cells stimulated by palmitic acid (PA). This disrupts its nucleocytoplasmic transport, impairs its transcriptional activity, and promotes obesity and type 2 diabetes [21]. SGs have also been reported to facilitate lipid droplet formation under starvation stress [22]. Consistent with these reports, we observed SG formation in MASH models. These results suggest that targeting G3BP1 and SG regulation may be a promising therapeutic strategy for MASH.

*Isodon lophanthoides* (Buch.-Ham. ex D. Don) Hara, a traditional Chinese medicinal herb, is widely used to treat acute hepatitis, acute cholecystitis, bruises, and swelling [23]. Diterpenoids are among its major bioactive constituents and exhibit cytotoxic, anti-inflammatory, antibacterial, and antioxidant activities [24-26]. Micranthin B (MB), a diterpenoid isolated from *I. lophanthoides*, has been studied for its anti-hepatocellular carcinoma properties [27, 28]. However, its effects on MASH remain poorly understood. In this study, we utilized a high-throughput drug screening model based on G3BP1 expression and identified MB as a compound that suppresses G3BP1 expression and shows anti-MASH activity. MB inhibited SG formation and alleviated MASH in both PA-stimulated cellular models and high-fat, high-cholesterol (HFHC) diet-fed mouse models. Mechanistically, MB directly targeted G3BP1, inhibited SG formation, prevented the recruitment of N-glycosylation-related proteins into SGs, restored N-glycosylation, and alleviated ER stress. MB also suppressed SG formation by inhibiting histone deacetylase 6 (HDAC6)-mediated deacetylation of G3BP1 under metabolic stress.

## 2. Materials and methods

### 2.1. Materials and reagents

Micranthin B (purity > 97%) was extracted and isolated from *I. lophanthoides* and subsequently characterized in our laboratory. Cycloheximide (CHX, Cat# HY-12320) were obtained from MedChemExpress. The primary and secondary antibodies used in this study were as follows: Actin (Proteintech, Cat# 81115-1-RR; Western Blotting (WB)), G3BP1 (Proteintech, Cat# 66486-1-Ig; co-immunoprecipitation [Co-IP] and WB), TIA1 (Abcam, Cat# ab140595; WB), Acetylated-Lysine (Cell Signaling Technology, Cat# 9441; WB), Myc-tag (ABclonal, Cat# AE010; WB), ATF4 (Abcam, Cat# ab270980; WB), BIP (ABclonal, Cat# A23453, used for WB), SEC61B (ABclonal, Cat# A21807, used for WB and Co-IP), CANX (ABclonal, Cat# A4846; WB and Co-IP), UGGT1 (ABclonal, Cat# A4866; WB), CALR (ABclonal, Cat# A20986; WB), LMAN1 (ABclonal, Cat# A4941; WB), Peroxidase Affinipure Goat Anti-Rabbit IgG (H + L) (YEASEN, Cat# 33101ES; WB), and Peroxidase Affinipure Goat Anti-Rabbit IgG (H + L) (YEASEN, Cat# 33201ES60; WB).

### 2.2. Animal studies

Eight-week-old male C57BL/6J mice (GemPharmatech Co., China) were housed under controlled conditions (23 ± 2 °C, 12 h light/dark cycle) with free access to standard laboratory chow and water. After a one-week acclimatization period, experiments commenced. For acute toxicity evaluation, mice received MB (300 $mg \cdot kg^{-1}$) or vehicle by oral gavage and were observed for 14 days. In the pharmacological study, a 16-week HFHC (14% protein, 42% fat, 44% carbohydrates and 0.2% cholesterol; Trophic, TP26304) diet-induced model was employed. From week 10 onward, mice received daily administration of MB (15 or 30 $mg \cdot kg^{-1}$) or obeticholic acid (OCA; 20 $mg \cdot kg^{-1}$) for six weeks while HFHC feeding continued. Control mice were fed normal chow (NC) (Q031; Shanghai Shilin Biologic Science & Technology). All animal experiments were approved by the Animal Ethics Committee at China Pharmaceutical University (No. 2022-03-018).

### 2.3. Cell lines

L02 cells (Chinese Academy of Sciences Cell Bank) were maintained in DMEM containing 10% FBS and 1% penicillin/streptomycin at 37 °C with 5% $CO_2$. To establish stable expression of G3BP1-EGFP in L02 cells, the G3BP1-EGFP plasmid was transfected into the cells, followed by selection with 900 $\mu g \cdot mL^{-1}$ of G418 after 48 h for 2 to 4 days. From days 10 to 14, selection continued with high-concentration G418 until week 4, when the concentration was reduced by half. Fluorescence microscopy revealed scattered green fluorescent cells, from which uniformly fluorescent single clones were isolated, expanded, and analyzed for G3BP1 expression. To evaluate the effects of MB on MASH-related changes, cells were exposed to PA (0.4 $mmol \cdot L^{-1}$) for 16 h and then treated with DMSO (vehicle control) or MB (5, 10, and 20 $\mu mol \cdot L^{-1}$) for 24 h.

### 2.4. Isolation and culturing of primary hepatocytes

Primary hepatocytes were enzymatically isolated from male C57BL/6J mice *via* collagenase perfusion. Following portal vein perfusion for blood clearance, livers were digested with 0.5 $mg \cdot mL^{-1}$ collagenase-I (Gibco) at 37 °C, mechanically dissociated, and filtered through 70 μm sieves. After centrifugation (50 g, 2 min, 4 °C), the hepatocytes were resuspended in complete DMEM. Lipid accumulation was induced by 16-h treatment with 0.4 $mmol \cdot L^{-1}$ PA complexed with 0.1% fatty acid-free BSA.

### 2.5. Glucose tolerance test (GTT) and insulin tolerance test (ITT)

For the GTT, overnight-fasted mice received intraperitoneal glucose (2 $g \cdot kg^{-1}$) and blood glucose were monitored at 0, 15, 30, 60, and 120 min after injection. For the ITT, mice were fasted for 6 h and injected intraperitoneally with insulin (0.75 $U \cdot kg^{-1}$), followed by blood glucose measurements at defined intervals. Glucose tolerance and insulin tolerance were quantified by calculating the area under the curve (AUC).

### 2.6. Histopathological staining

Hepatic histopathology was assessed by hematoxylin and eosin (H&E) staining and Oil Red O staining (Wuhan Servicebio Technology, Wuhan, China). Tissue sections were microscopically examined (Olympus) and quantitatively analyzed using FIJI ImageJ.

### 2.7. Serum biochemical analysis

Serum alanine aminotransferase (ALT), aspartate aminotransferase (AST), total cholesterol (TC), and triglycerides (TG) levels in MASH models were measured using standardized assay kits (Nanjing Jiancheng Bioengineering Institute) as per manufacturer's instructions.

### 2.8. WB and Co-IP

Total protein was extracted from liver tissues and cells using lysis buffer (YESEN, 20118ES) containing protease inhibitors

(Beyotime, P1005). For WB, proteins were resolved by SDS-PAGE, transferred to PVDF membranes, and immunoprobed. Signals were detected with Bio-Rad ECL (170-5061) and quantified using FIJI ImageJ. For Co-IP, lysates were incubated with target antibodies and Protein A/G beads (4 °C, overnight), washed, and eluted in SDS buffer. Clean-Blot IP Reagent (Thermo Fisher, 21230) served as secondary antibody to minimize IgG interference.

### 2.9. Quantitative RT-PCR

Total RNA was isolated from liver tissues and cells and reverse-transcribed into cDNA. Quantitative PCR analysis was conducted using SYBR Green Master Mix (Vazyme, Q321-02), with target gene mRNA levels normalized to housekeeping genes (*Actin* or *GAPDH*). Primer sequences are listed in Table S1.

### 2.10. Plasmid constructs

The human G3BP1 coding sequence was cloned into both pCMV-N-Myc and pcDNA3 APEX2-NES vectors using conventional subcloning methods. The pCMV-N-Myc vector was obtained from Beyotime, and the pcDNA3 APEX2-NES vector was sourced from Addgene. G3BP1 mutants S149E, S149A, and K376Q were generated using the Mut Express kit (Vazyme) by site-directed mutagenesis. Primer sequences for plasmid construction are provided in Table S2.

### 2.11. Immunofluorescence and lipid droplet staining

For G3BP1-EGFP immunofluorescence, L02 cells underwent PBS washes nd stained with Hoechst for nuclear visualization. For lipid droplet staining, fixed cells were labeled with 0.5 μmol·L$^{-1}$ BODIPY (4,4-difluoro-3a,4a-diaza-s-indacene; 493/503, Invitrogen, D3922) and imaged by confocal microscopy (ImageXpress) using identical settings across all groups. Fluorescence intensity was quantified using FIJI ImageJ.

### 2.12. Small interfering RNA transfection

L02 cells were transfected with G3BP1-specific siRNA (5′-CAAAUCAGAGCUUAAAGAU-3′) or HDAC6-specific siRNA (5′-GGATGGATCTGAACCTTGAGA-3′) (Ribobio, Guangzhou). Following transfection in complete medium, the cells were subjected to the aforementioned treatments.

### 2.13. RNP granule fractionation

Cells cultured in 10 cm dishes were rinsed with cold PBS, followed by lysis in 1 mL of buffer L (50 mmol·L$^{-1}$ Tris, pH 7.6, 50 mmol·L$^{-1}$ NaCl, 5 mM $MgCl_2$, 0.1% NP-40, and 1 mmol·L$^{-1}$ β-mercaptoethanol), supplemented with EDTA-free protease and phosphatase inhibitors. Whole-cell lysates were centrifuged at 2000 g for 5 min to remove nuclei. RNP granules were fractionated from the supernatant by centrifugation at 10 000 *g* for 10 min. The supernatant was designated as the soluble fraction. The pellet, after three washes with buffer L, was collected as the RNP granule (RG) fraction. Protein concentrations were quantified by BCA assay, and samples were denatured in loading buffer for immunoblotting.

### 2.14. Drug affinity responsive target stability (DARTS) and cell thermal shift assay (CETSA)

The DARTS assay was performed to assess drug-protein binding stability [29]. After lysis in NP-40 buffer (MedChemExpress) and centrifugation at 15 000 *g* for 10 min at 4 °C, cell lysates were incubated with MB (0, 5, 10, and 20 μmol·L$^{-1}$) at 37 °C for 1 h in a ThermoMixer C (Eppendorf). Pronase (1∶100) was then added, and the lysates were incubated (37 °C, 30 min) to digest proteins. The reaction was quenched with PMSF and incubated on ice for 10 min. Western blot analysis was performed to assess protein stability. The CETSA assay was adapted from the literature [30]. L02 cells were exposed to 20 μmol·L$^{-1}$ MB or DMSO for 6 h. After collection and PBS washing (containing PMSF), cells were equally divided into eight tubes. Each tube was incubated at 40, 44, 48, 52, 56, 60, 64, and 68 °C for 3 min using a Mastercycler nexus GX2 (Eppendorf). The cells were then subjected to three liquid nitrogen/room temperature freeze-thaw cycles and centrifuged (15 000 *g*, 10 min, 4 °C). Supernatants were collected for immunoblot analysis.

### 2.15. APEX-mediated biotinylation

APEX2-G3BP1-transfected L02 cells were treated with 0.4 mmol·L$^{-1}$ PA or BSA for 16 h. Biotinylation was initiated by adding 500 μmol·L$^{-1}$ biotin-phenol and incubating the cells at 37 °C for 30 min. The reaction was then triggered by 1 mmol·L$^{-1}$ $H_2O_2$ for 1 min. To quench biotinylation, Trolox (5 mmol·L$^{-1}$, Sigma 238813) and sodium ascorbate (10 mmol·L$^{-1}$, Sigma A4034) were added. For enrichment of biotinylated proteins, 2–4 mg protein was incubated with 100 μL streptavidin magnetic beads (Invitrogen, Cat# 65305) at room temperature for 2 h. Beads were sequentially washed with RIPA buffer and 2 mol·L$^{-1}$ urea in 10 mmol·L$^{-1}$ Tris-HCl (pH 8.0) before mass spectrometry (MS) analysis.

### 2.16. RNA sequencing (RNA-seq) analysis

Total RNA was extracted and reverse-transcribed into cDNA for the construction of an indexed Illumina sequencing library. RNA-seq of L02 cells was performed in collaboration with Novogene (Beijing, China). Raw sequencing data were analyzed using the NovoMagic platform for enrichment studies. A $P$-value < 0.05 defined statistical significance.

### 2.17. Statistical analysis

Data were analyzed using GraphPad Prism 9 (GraphPad Software). Error bars represent the standard error of the mean (SEM). Two-tailed *t*-tests were used for two-group comparisons, and one-way ANOVA with Tukey's post hoc analysis was used for multiple-group comparisons. Statistical significance was set at $P$ < 0.05.

## 3. Results

### 3.1. High-content screening identifies compounds that modulate G3BP1

Previous studies have shown that G3BP1 protein levels are elevated in HCC tissues [18, 31]. Because MASH is a well-recognized risk factor for HCC, we first examined whether G3BP1 is also dysregulated in MASH. We found that G3BP1 protein levels were markedly increased in both MASH cells and mouse models (Figs. S1A and S1B). To explore the potential natural product regulating G3BP1, we conducted a high-content screening using an L02 cell line stably overexpressing G3BP1-EGFP and evaluated 430 natural compounds (Figs. 1A and 1B). The G3BP1-EGFP cell line exhibited stable G3BP1 expression, and G3BP1 knockdown markedly reduced the G3BP1-EGFP signal, confirming the validity of the screening system (Fig. S1C). We observed that MB, isolated from *I. lophanthoides*, significantly reduced the fluorescence intensity of G3BP1-EGFP (Figs. 1B–1D). To determine suitable concentrations for subsequent experiments, we assessed the

cytotoxic effects of MB in L02 cells (Fig. S1D). MB significantly inhibited the PA-induced upregulation of G3BP1 in a concentration-dependent manner in L02 cells and primary hepatocytes (Figs. 1E and 1F). In addition, DARTS and CETSA experiments confirmed the binding of MB to G3BP1 (Figs. 1G and 1H).

### 3.2. MB significantly alleviates MASH progression

We next evaluated the anti-MASH activity of MB *in vitro* and in *vivo*. MB attenuated PA-induced lipid accumulation in L02 cells, as shown by BODIPY and Oil Red O staining (Figs. 2A and S2A). The mRNA levels of *IL-6*, *IL-1β*, and *TNF-α* were also downregulated following MB treatment in L02 cells (Fig. S2B). These results indicate that MB effectively ameliorates MASH-like changes *in vitro*. Before evaluating its efficacy *in vivo*, we first evaluated the safety of MB by use of a single maximum-dose administration method. After oral gavage of MB at 300 mg·kg$^{-1}$ and a 14-day observation period, no significant abnormalities were observed in behavior, skin, mental state, or excreta in comparison with the control group. H&E staining showed that high-dose MB had no impact on the histopathological structure of the heart, liver, spleen, lungs, or kidneys, indicating that MB had no obvious organ toxicity and exhibits good *in vivo* safety (Fig. 2B). To further investigate its therapeutic effects, we established a mouse MASH model induced by an HFHC diet and administered MB (15 or 30 mg·kg$^{-1}$) or OCA (20 mg·kg$^{-1}$) *via* oral gavage (Fig. 2C). Following 16 weeks of HFHC feeding, the liver-to-body weight ratio was significantly increased in the HFHC group, whereas treatment with MB and OCA markedly attenuated this increase (Fig. 2D). Additionally, improved insulin sensitivity and reduced lipid deposition were observed in the MB- and OCA-treated groups (Figs. 2E, S2C, and S2D). We found significantly lower serum TC and TG, as well as ALT and AST levels, in the MB- and OCA-treated groups (Figs. 2F and 2G). MB increased the expression of genes involved in fatty acid β-oxidation and reduced the expression of genes related to fatty acid uptake and synthesis (Fig. 2H). MB- and OCA-treated mice also showed improved inflammatory responses, as indicated by cytokine gene expression (Fig. 2H). These results indicate that MB has a beneficial effect on MASH mice.

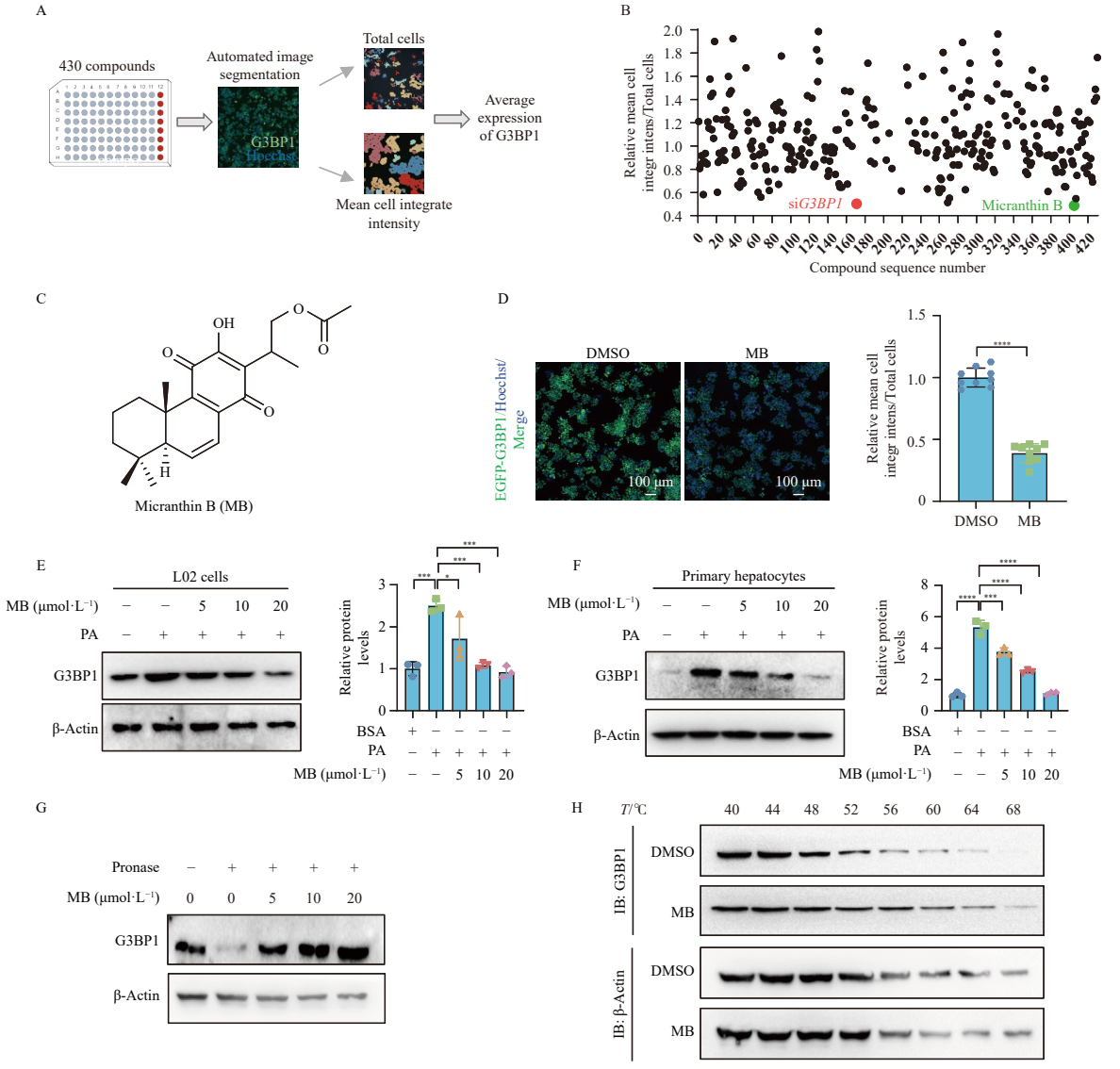


**Fig. 1** High-content screening identifies MB as a potent modulator of G3BP1. (A and B) Schematic overview of the screening workflow (A) and distribution of fluorescence intensity in L02 cells stably expressing G3BP1-EGFP after treatment with 430 compounds (B). (C) Chemical structure of MB. (D) Representative fluorescence images and quantification of G3BP1-EGFP intensity in MB-treated L02 cell line stably expressing G3BP1-EGFP. Average fluorescence intensity per cell was quantified. $n$ = 9 ROIs from 3 independent experiments. (E and F) WB analysis and quantification of G3BP1 expression in PA-stimulated (0.4 mmol·L$^{-1}$, 16 h) L02 cells (E) and primary hepatocytes (F) following treatment with MB (5, 10, and 20 μmol·L$^{-1}$) or DMSO for 24 h. $n$ = 3 independent experiments per group. (G and H) CETSA (G) and DARTS (H) analyses of MB binding to G3BP1. Data are presented as mean ± SEM, $^{*}P < 0.05$, $^{**}P < 0.01$, $^{***}P < 0.001$, $^{****}P < 0.0001$.

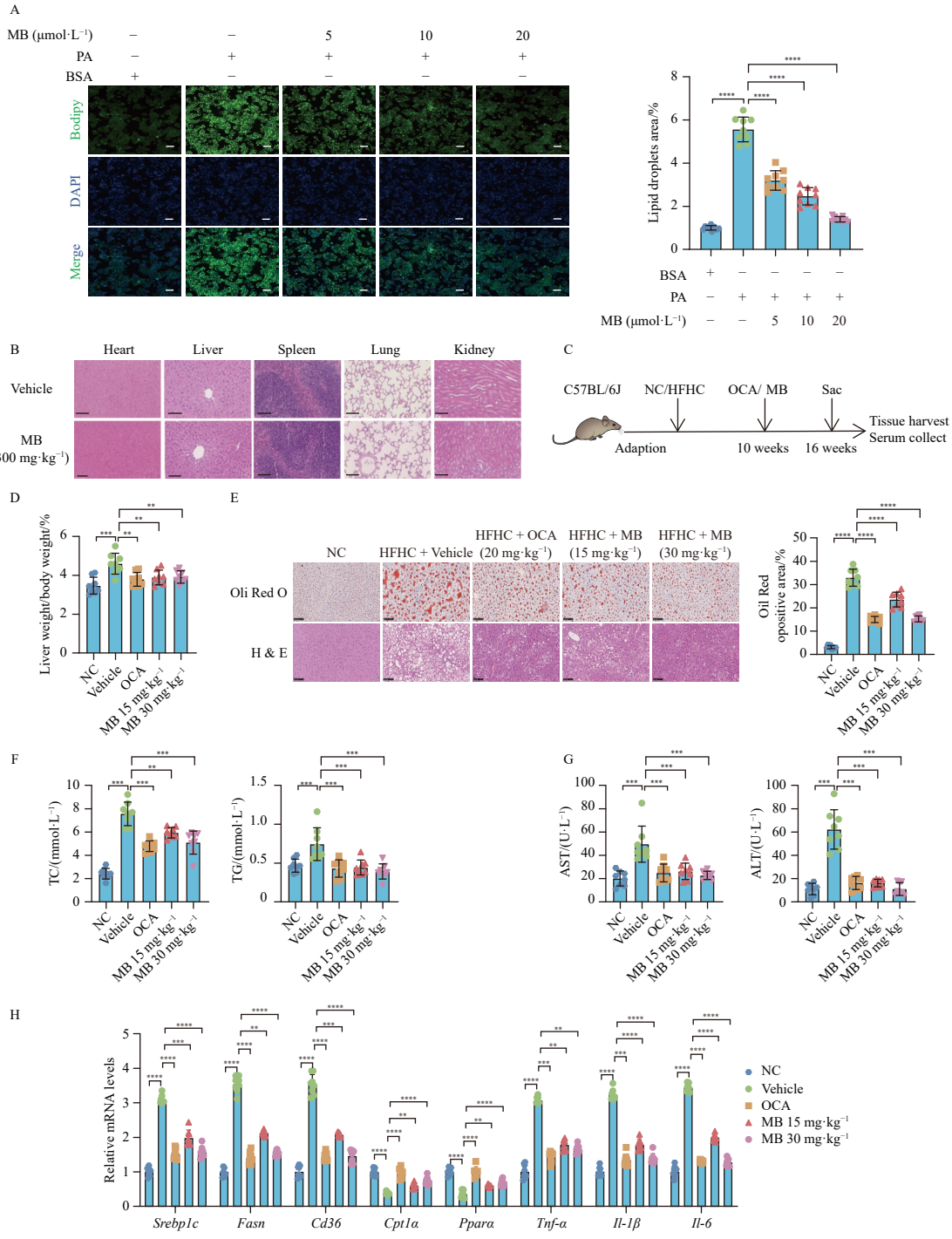


**Fig. 2** MB significantly alleviates MASH progression. (A) BODIPY staining and quantification in L02 cells treated with MB (5, 10, and 20 μmol·L$^{-1}$) or DMSO for 24 h. Scale bars, 100 μm. Average fluorescence intensity per cell was quantified. $n$ = 9 ROIs from 3 independent experiments. (B) H&E staining of the heart, liver, spleen, lungs, and kidneys in mice following a single maximum-dose administration of MB (300 mg·kg$^{-1}$). Scale bars, 100 μm. (C and D) Schematic overview of the experimental design (C) and liver-to-body weight ratio (D) in NC- or HFHC-fed mice administered MB (15 or 30 mg·kg$^{-1}$), OCA (20 mg·kg$^{-1}$), or vehicle by oral gavage for six weeks ($n$ = 6 mice/group). (E) H&E staining, Oil red O staining, and quantification of liver sections in the indicated groups ($n$ = 6 mice/group). Scale bars, 100 μm. (F and G) Serum levels of TC, TG, ALT, and AST in the indicated groups ($n$ = 6 mice/group). (H) Relative mRNA expression of genes related to fatty acid synthesis, fatty acid uptake, fatty acid β-oxidation, and inflammation in the indicated groups ($n$ = 6 mice/group). Data are presented as mean ± SEM, $^{*}P < 0.05$, $^{**}P < 0.01$, $^{***}P < 0.001$, $^{****}P < 0.0001$.

### 3.3. MB improves N-glycosylation and alleviates ER stress

To investigate how MB ameliorates MASH, we conducted RNA-seq employing PA-induced L02 cells and compared the MB-treated group (20 μmol·L$^{-1}$) with the solvent-treated control group. We identified a total of 1315 differentially expressed genes (DEGs; Table S3). Kyoto Encyclopedia of Genes and Genomes (KEGG) and Gene Ontology (GO) pathway enrichment analyses were then performed. GO analysis revealed that MB primarily affected functions related to the ER, including SRP-dependent cotranslational protein targeting to the membrane, protein targeting to the ER, establishment of protein localization to the ER, and protein localization to the ER (Fig. 3A). KEGG enrichment analysis indicated that functions related to N-glycosylation, including N-glycan biosynthesis and various types of N-glycan biosynthesis, underwent significant changes (Fig. 3B). Consistently, we observed significant differential expression of N-glycosylation-related genes, including *ALG10B*, *DAD1*, *FUT8*, *MAN1A2*, *MAN2A1*, and *CALR* (Table S3). Because N-glycosylation mainly occurs in the ER [11], we further examined genes involved in this process. N-

glycosylation was significantly inhibited in the livers of HFHC diet-fed mice, whereas MB treatment effectively reversed this inhibition (Fig. 3C). A similar improvement was observed in MB-treated PA-stimulated L02 cells (Fig. S3A). Because N-glycosylation assists in the proper folding of proteins, abnormal glycosylation can lead to the accumulation of misfolded proteins and activation of ER stress [32]. Accordingly, MB significantly suppressed the expression ER stress-related genes and proteins in HFHC-fed mouse livers and PA-stimulated L02 cells (Figs. 3D, 3E, S3B, and S3C). Taken together, these data suggest that MB ameliorates MASH by enhancing N-glycosylation and alleviating ER stress.

### 3.4. MB targets G3BP1 to modulate N-glycosylation and ER stress

Next, we investigated whether the mitigation of MASH by MB depends on G3BP1. We observed a significant improvement in N-glycosylation following G3BP1 knockdown in PA-stimulated L02 cells (Fig. 4A). Concurrently, ER-related gene expression was markedly downregulated, indicating an alleviation of ER stress (Fig. 4B). In contrast, the inhibited N-glycosylation process and exacerbated ER stress were observed in PA-stimulated L02 cells with G3BP1 overexpression (Figs. 4C–4E). These results suggest that G3BP1 inhibits N-glycosylation, thereby promoting ER stress. We further assessed the impact of MB on N-glycosylation and ER stress in PA-stimulated primary hepatocytes and L02 cells, with or without G3BP1 overexpression. G3BP1 overexpression reversed the effects of MB on the enhancement of N-glycosylation and the alleviation of ER stress (Figs. 4F–4I). These findings suggest that MB mitigates N-glycosylation and ER stress by targeting G3BP1.

### 3.5. MB disrupts SG formation to alleviate ER stress

G3BP1 is a core component of SG and is essential for their formation [19, 20]. Immunofluorescence results showed that SGs were predominantly formed in PA-treated L02 cells, while MB treatment significantly inhibited SG formation (Fig. 5A). Therefore, we hypothesized that the effects of MB on N-glycosy-

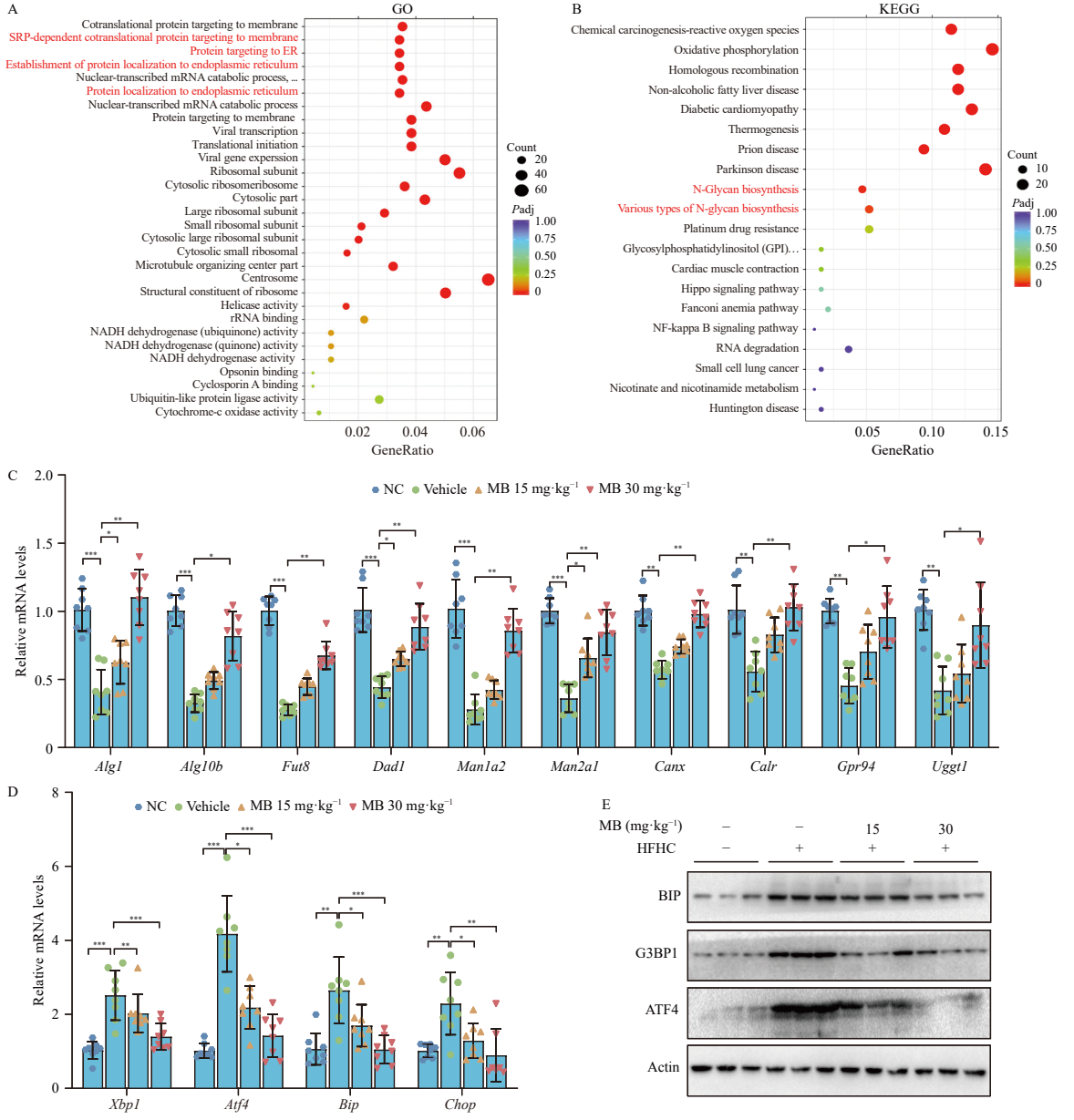


**Fig. 3** MB improves N-glycosylation and alleviates ER stress. (A and B) GO (A) and KEGG pathway (B) analyses of DEGs in PA-stimulated L02 cells with or without MB treatment. (C) Relative mRNA expression of genes associated with N-glycosylation synthesis in HFHC- or NC-fed mice administered MB (15 or 30 mg·kg$^{-1}$) or vehicle by oral gavage for six weeks ($n$ = 6 mice/group). (D) Relative mRNA expression of ER stress-related genes in the indicated groups ($n$ = 6 mice/group). (E) WB analysis of ER stress-related protein expression in the indicated groups. Data are presented as means ± SEM, $^{*}P < 0.05$, $^{**}P < 0.01$, $^{***}P < 0.001$, $^{****}P < 0.0001$.

lation and ER stress may be associated with SGs. To test this possibility, we evaluated N-glycosylation and ER stress after disrupting SG formation. We generated G3BP1 mutants, G3BP1-S149A and G3BP1-S149E, by altering the charge content of the IDR1 region. It has been reported that the phosphomimetic form (S149E) reduces SG formation, whereas the non-phosphorylatable form (S149A) maintains the original charge state [20]. In our study, the G3BP1-S149E variant significantly enhanced N-glycosylation and inhibited ER stress in PA-treated primary hepatocytes and L02 cells (Figs. 5B–5G). Additionally, the SG inhibitor CHX [33] significantly increased N-glycosylation and inhibited ER stress in both PA-treated primary hepatocytes and L02 cells (Figs. S4A–S4F). Therefore, we conclude that G3BP1 inhibits N-glycosylation and promotes ER stress in an SG-dependent manner, and that MB alleviates MASH by inhibiting SG formation.

### *3.6. SGs recruit N-glycosylation-related proteins and promote ER stress*

Aberrant SG formation can cause excessive sequestration of proteins, thereby disrupting cellular stress responses and impairing their proper function [33, 34]. As SG formation inhibited N-glycosylation, in our models, we hypothesized that SGs may recruit N-glycosylation-related proteins and thereby interfere with their activity. To confirm this hypothesis, we employed ascorbate peroxidase (APEX)-mediated proximity labeling in combination with quantitative MS [35] to characterize the SG-associated proteome under PA stimulation (Fig. 6A). APEX fused to G3BP1 was introduced into L02 cells, which were subsequently stimulated with either BSA or PA. After APEX activation with biotin tyramide and $H_2O_2$, G3BP1-associated proteins were enriched using streptavidin agarose and analyzed by MS. Compared with BSA treatment, five N-glycosylation-related proteins were differentially enriched in the PA-treated group: SEC61B, UGGT1, CANX, CALR, and LMAN1 (Fig. 6A and Table S4).

To further provide biochemical evidence for the association between N-glycosylation-related proteins and SGs, both soluble cytoplasmic lysates and insoluble RNP granules containing SGs were isolated by differential centrifugation. The results indicated

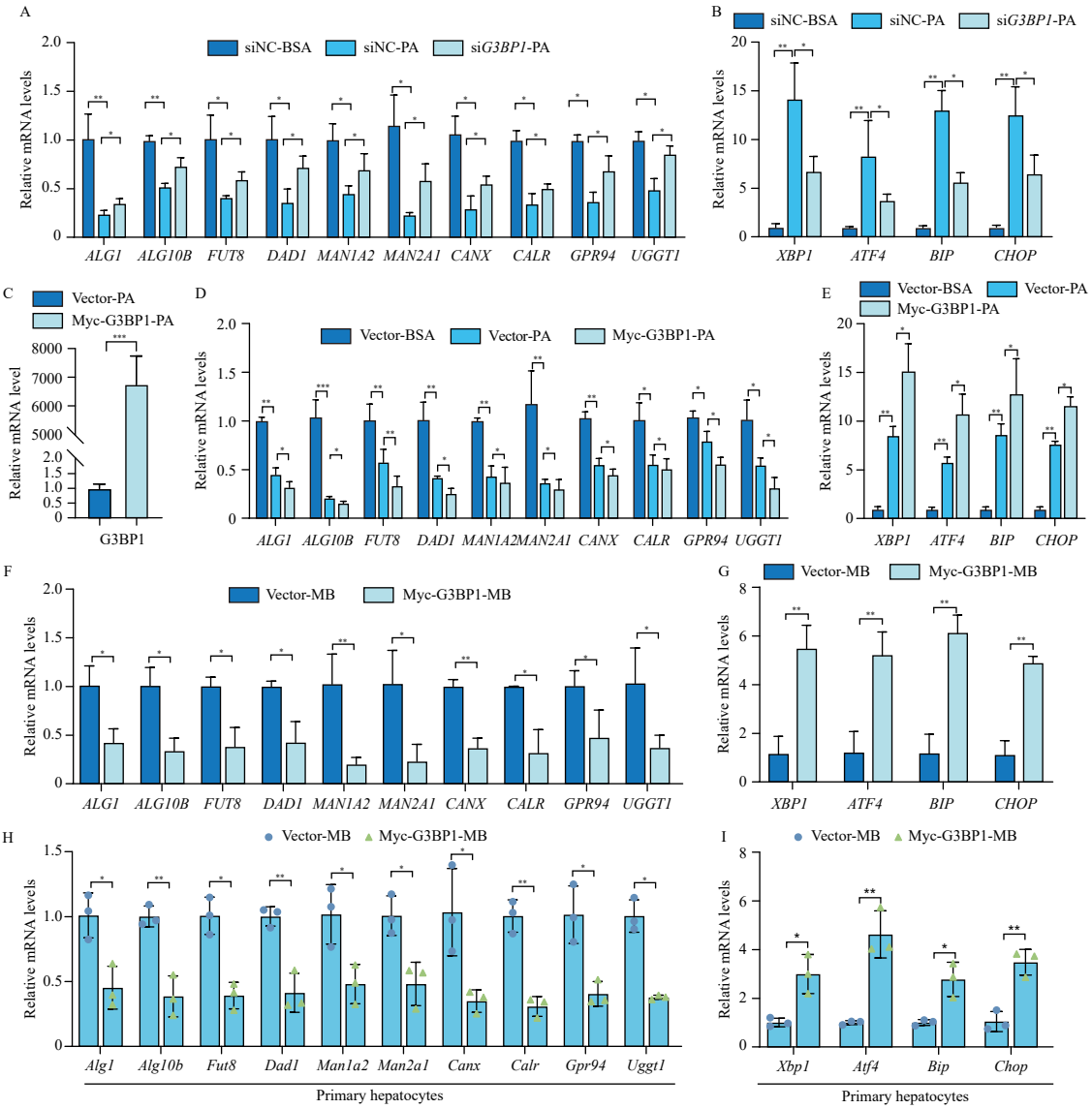


**Fig. 4** MB regulates N-glycosylation and ER stress through G3BP1. (A and B) Relative mRNA expression of genes associated with N-glycosylation (A) and ER stress (B) in L02 cells infected with si*G3BP1* followed by BSA or PA (0.4 mmol·L$^{-1}$,16 h) treatment. $n$ = 3 independent experiments per group. (C) Relative mRNA expression levels of G3BP1 in L02 cells transfected with or without Myc-G3BP1 followed by PA (0.4 mmol·L$^{-1}$, 16 h) treatment. $n$ = 3 independent experiments per group. (D and E) Relative mRNA expression levels of genes associated with N-glycosylation (D) and ER stress (E) in L02 cells transfected with Myc-G3BP1 followed by BSA or PA treatment. $n$ = 3 independent experiments per group. (F–I) Relative mRNA expression levels of genes associated with N-glycosylation and ER stress in L02 cells or primary hepatocytes transfected with Myc-G3BP1 followed by MB (20 μmol·L$^{-1}$, 24 h) treatment. $n$ = 3 independent experiments per group. Data are presented as means ± SEM, $^{*}P < 0.05$, $^{**}P < 0.01$, $^{***}P < 0.001$, $^{****}P < 0.0001$.

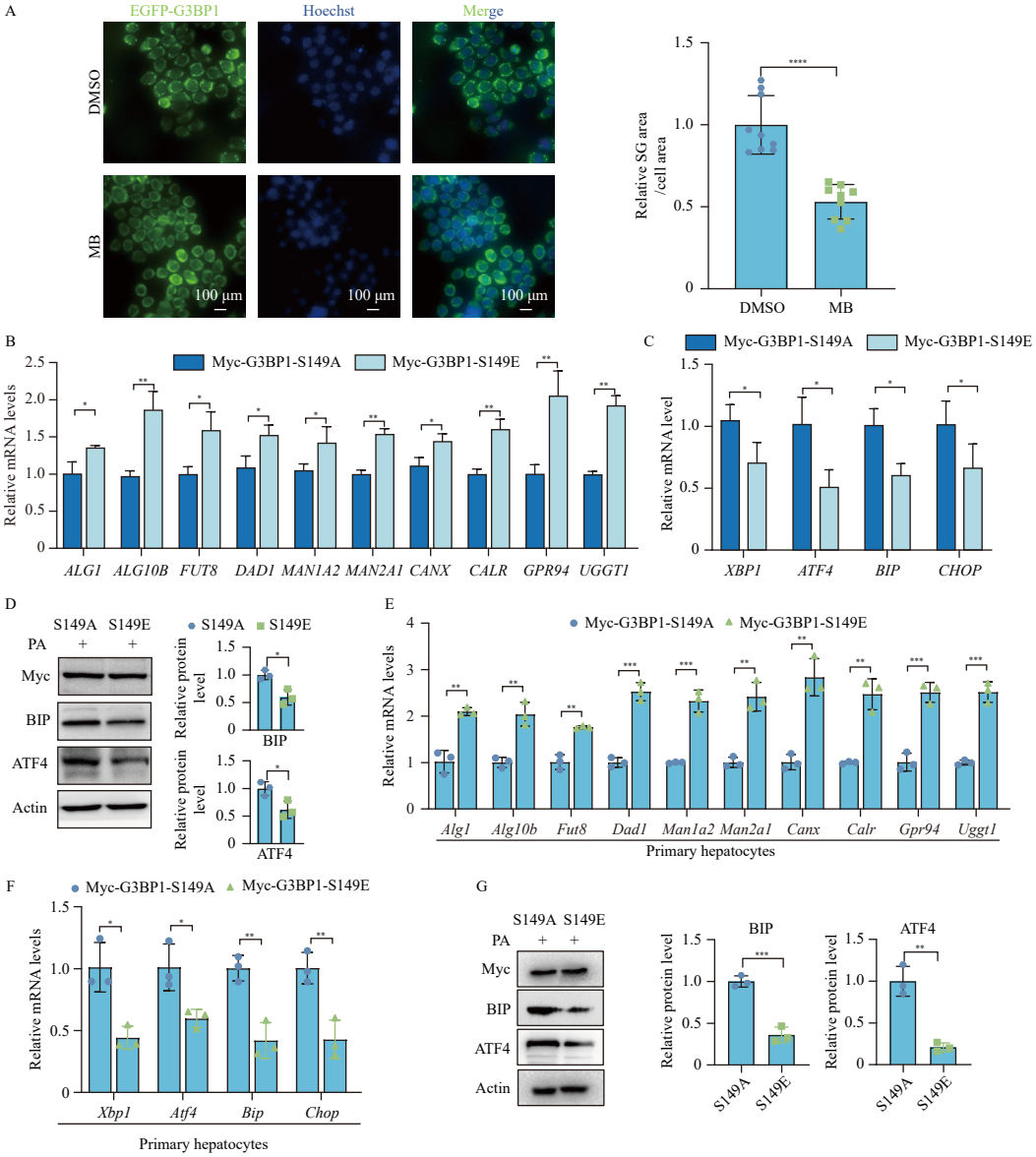


**Fig. 5** MB disrupts SG formation and alleviates ER stress. (A) Representative images showing SG assembly in PA-stimulated (0.4 mmol·L$^{-1}$, 16 h) L02 cells following treatment with DMSO or MB (20 μmol·L$^{-1}$, 24 h). The relative SG area per cell was quantified ($n$ = 9 ROIs from three independent experiments). (B and C) Relative mRNA expression levels of genes associated with N-glycosylation (B) and ER stress (C) in PA-stimulated (0.4 mmol·L$^{-1}$, 16 h) L02 cells transfected with Myc-G3BP1-S149A or Myc-G3BP1-S149E. $n$ = 3 independent experiments per group. (D) WB analysis of ER stress-related protein expression in the indicated groups. $n$ = 3 independent experiments per group. (E and F) Relative mRNA expression levels of genes associated with N-glycosylation (E) and ER stress (F) in primary hepatocytes in the indicated groups. $n$ = 3 independent experiments per group. (G) WB analysis of ER stress-related protein expression in the indicated groups. $n$ = 3 independent experiments per group. Data are presented as means ± SEM, $^{*}P < 0.05$, $^{**}P < 0.01$, $^{***}P < 0.001$, $^{****}P < 0.0001$.

that SG recruited two N-glycosylation-related proteins, SEC61B and CANX, in both PA-stimulated L02 cells and primary hepatocytes (Figs. 6B and 6C). SGs induced by other stressors, including $NaAsO_2$, $H_2O_2$, and heat shock, similarly recruited these proteins (Figs. 6B and 6C). However, MB treatment, which inhibited SG formation in PA-stimulated L02 cells and primary hepatocytes, significantly reduced the recruitment of SEC61B and CANX into SGs (Figs. 6D and 6E). N-glycosylation is initiated by two multisubunit OST complexes, OST-A and OST-B [13, 36]. During co-translational glycosylation, OST-A anchors the glycan to the SEC61 protein channel, allowing glycosylation of nascent polypeptides as they emerge from SEC61 [12, 13]. Co-IP assays revealed that metabolic stress reduced the interaction between SEC61B and OST-A catalytic subunit STT3A after SG formation, which was subsequently restored by MB treatment (Fig. 6F). CANX, an ER membrane protein, is mainly responsible for the correct folding of proteins after N-glycosylation [37] and functions through interaction with protein disulfide isomerase family A member 3 (PDIA3/ERp57), forming the calnexin cycle [14, 15]. When protein folding errors occur, misfolded proteins accumulate, leading to ER stress [37]. Co-IP experiments demonstrated that metabolic stress reduced the interaction between CANX and ERp57 after SG formation, whereas this effect was reversed by MB treatment (Fig. 6G). Overall, these results further demonstrate that, under stress conditions, SG formation sequesters SEC61B and CANX, impairs their functions in N-glycosylation and protein folding, and thereby promotes ER stress and MASH progression. MB alleviates these effects by inhibiting SG formation.

### *3.7. MB inhibits SG formation by suppressing HDAC6-mediated deacetylation of G3BP1*

MB targeting G3BP1 and inhibiting SG formation prompted us to investigate how MB regulated the function of G3BP1. SG assembly and disassembly are highly dynamic processes controlled by intracellular regulation of protein translation and RNA metabolism [38, 39]. Research indicates that G3BP1 acetylation is involved in SG assembly [40]. The Co-IP data demonstrated a signific-

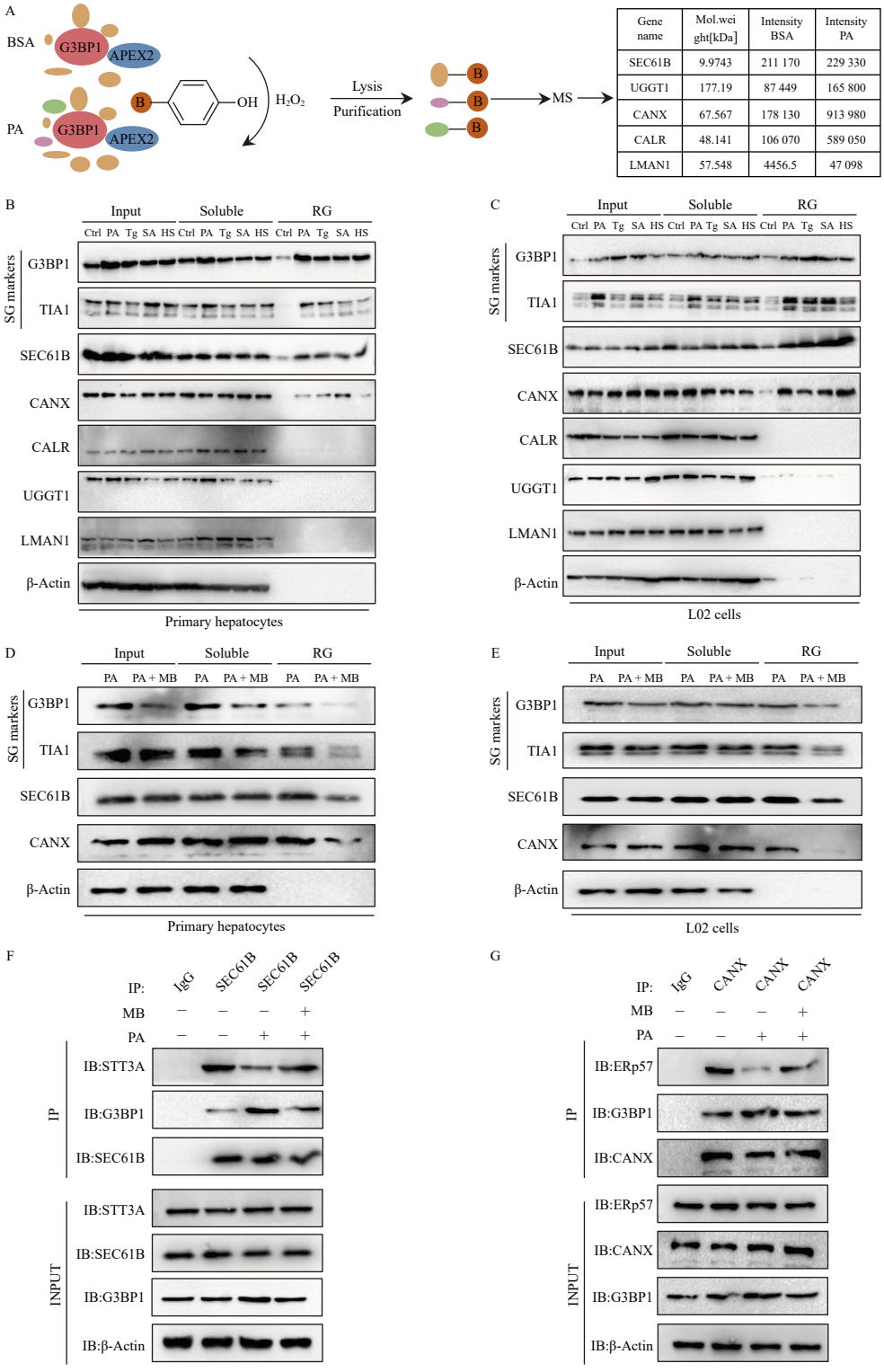


| Gene name | Mol.weight[kDa] | Intensity BSA | Intensity PA |
|---|---|---|---|
| SEC61B | 9.9743 | 211 170 | 229 330 |
| UGGT1 | 177.19 | 87 449 | 165 800 |
| CANX | 67.567 | 178 130 | 913 980 |
| CALR | 48.141 | 106 070 | 589 050 |
| LMAN1 | 57.548 | 4456.5 | 47 098 |

**Fig. 6** SG recruits N-glycosylation-related proteins, impair N-glycosylation, and induce ER stress. (A) Schematic diagram of the APEX2 proximity-labeling experiment. (B and C) WB analysis of the indicated proteins in primary hepatocytes (B) and L02 cells (C) treated with Control, PA, Tg, SA, or HS. Input: whole-cell lysates; Soluble: the soluble fraction excluding the nucleus; RG: the insoluble RG fraction. Actin was used as a loading control. (D and E) WB analysis of the indicated proteins in primary hepatocytes (D) and L02 cells (E) treated with MB (20 μmol·$L^{-1}$, 24 h). (F and G) Co-IP and WB analysis of the indicated proteins in PA-stimulated L02 cells treated with or without MB (20 μmol·$L^{-1}$, 24 h).

ant reduction in G3BP1 acetylation levels, which was accompanied by a marked increase in MB-treated L02 cells under PA stimulation (Fig. 7A). This suggests that MB may regulate SG formation through modulating G3BP1 protein.

Acetylation of G3BP1 at K376 has been reported to inhibit SG formation, providing a potential avenue to mitigate excessive stress responses under pathological conditions [40]. We therefore constructed Myc-tagged wild-type G3BP1 and the acetylation-mimetic mutant G3BP1-K376Q. Co-IP results showed that MB significantly reduced the acetylation level of G3BP1 WT but had no effect on the acetylation level of G3BP1 K376Q in PA-treated L02 or primary hepatocytes (Figs. 7B, 7C, S5A, and S5B). HDAC6 is known to regulate the acetylation of G3BP1 [40]. We found that HDAC6 knockdown actually increased G3BP1 acetylation levels (Figs. 7D and S5C). Co-IP results indicated that MB disrupted the interaction between G3BP1 and HDAC6 (Fig. 7E), suggesting that

MB binds to G3BP1 and prevents HDAC6-mediated deacetylation. Functionally, MB significantly reversed the decline in N-glycosylation and the increase in ER stress caused by WT-G3BP1 overexpression, while exhibiting no significant effect on cells expressing the G3BP1-K376Q mutant (Figs. 7F, 7G, S5D, and S5E). In conclusion, these data suggest that MB disrupts HDAC6-mediated deacetylation of G3BP1, thereby inhibiting SG assembly and subsequently improving N-glycosylation and alleviating ER stress.

## 4. Dicussion

Target-based drug screening has emerged as a crucial strategy in the development of therapeutic interventions for MASH. In particular, natural compounds derived from traditional Chinese medicine provide a valuable source of potential lead compounds [41-45]. In this study, utilizing a high-throughput drug screening system based on G3BP1 expression levels, we identified MB, extracted and isolated from *I. lophanthoides*, as a compound that significantly ameliorates MASH by modulating ER homeostasis. Mechanistically, MB inhibited the expression of G3BP1 and SG formation. This prevented SG-mediated sequestration of the N-glycosylation-related proteins CANX and SEC61B, restored N-glycosylation, and reduced ER stress.

SGs are a class of important biomolecular condensates, in which G3BP1 serves as a core protein regulating their assembly through liquid-liquid phase separation (LLPS) [20]. A growing body of research suggests that dysregulation of SG components and aberrant SG assembly are involved in the pathogenesis of metabolic disorders, inflammation, and cancer [46, 47]. G3BP1 promotes tumor migration and proliferation in HCC patients, while forming SGs reduces HCC sensitivity to chemotherapeutic drugs [18, 48]. SG formation has also been detected in pancreatic β cells stimulated by PA [21]. Consistent with these findings, we observed increased G3BP1 expression and SG formation in both cellular and animal models of MASH. Therefore, targeting G3BP1 or modulating SG assembly may be a viable therapeutic strategy. Through high-throughput screening, we identified that the compound MB significantly inhibited the expression of G3BP1 and demonstrated notable ameliorative effects in both cellular and animal models of MASH. MB also significantly suppressed the formation of SGs. G3BP1 acetylation is known to regulate the assembly of SG, and HDAC6-mediated deacetylation of G3BP1 at lysine 376 (K376) promotes SG formation. In contrast, acetylation at this site disrupts the interaction of G3BP1 with its partner proteins (such as USP10, CAPRIN1, or PABP1), thereby inhibiting SG assembly [31, 40].

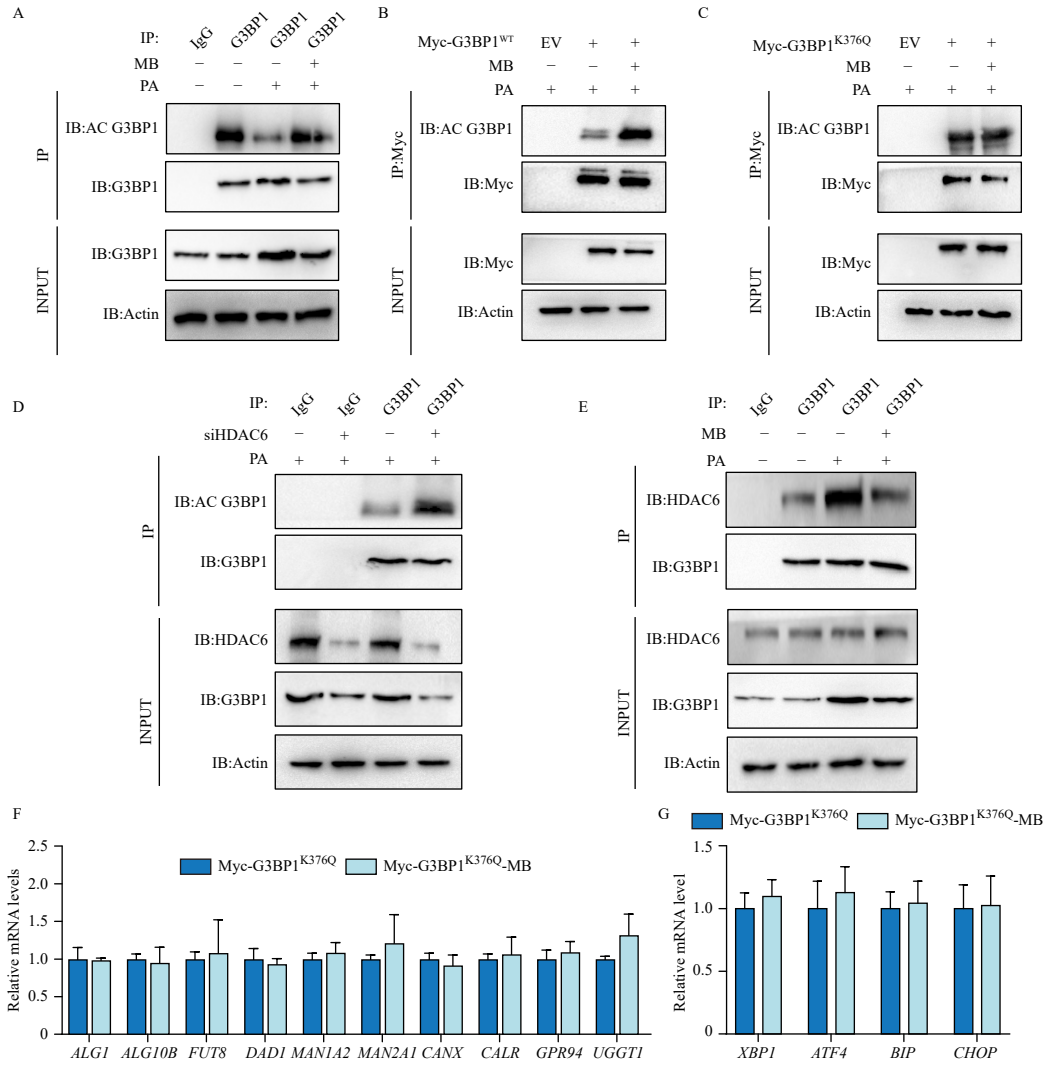


**Fig. 7** MB inhibits SG formation by suppressing HDAC6-mediated deacetylation of G3BP1. (A) Representative immunoblot of acetylated G3BP1 (Ac-G3BP1) in L02 cells treated with MB (20 μmol·L$^{-1}$, 24 h) or DMSO. (B and C) Representative immunoblots of Ac-G3BP1 in L02 cells transfected with Myc-G3BP1 (B) or Myc-G3BP1$^{K376Q}$ (C) and treated with or without MB (20 μmol·L$^{-1}$, 24 h). (D) Representative immunoblot of Ac-G3BP1 in L02 cells infected with si*HDAC6*. (E) Co-IP and WB analyses of the indicated proteins in PA-stimulated L02 cells treated with or without MB (20 μmol·L$^{-1}$, 24 h). (F and G) Relative mRNA expression levels of genes associated with N-glycosylation (F) and ER stress (G) in L02 cells infected with Myc-G3BP1 or Myc-G3BP1$^{K376Q}$ and treated with or without MB (20 μmol·L$^{-1}$, 24 h). $n$ = 3 independent experiments per group.

Consistently, we demonstrated that MB inhibited SG formation by disrupting HDAC6-mediated deacetylation of G3BP1 at K376.

N-linked glycosylation directs nascent glycoproteins toward proper folding, degradation, or export pathways [9, 49]. This process prevents unfolded glycoproteins from accumulating in the ER lumen and activates the UPR pathway. Genes related to N-glycan biosynthesis in the ER were found to significantly downregulated as MASLD progressed. Reduced expression of these genes impairs glycosylation of key transporters, disrupts their function, and promotes disease progression [10]. Additionally, altered N-glycan biosynthesis, including increased fucosylation, has been associated with fibrosis in NASH patients [50]. In this study, MB upregulated genes involved in N-glycan biosynthesis in both MASH mouse and cell models and simultaneously reduced ER stress. These findings support MB as a promising potential lead compound for treating MASH.

In addition, we further discovered that MB influenced N-glycosylation and ER stress through G3BP1. Currently, G3BP1 has been found to influence various cellular organelles. At the lysosomal cytoplasmic surface, G3BP1 inhibits mechanistic target of rapamycin complex 1 (mTORC1) activation by anchoring the tuberous sclerosis complex (TSC) protein complex to lysosomes [51]. It also interacts with mitochondrial $H^+$-ATP synthase subunit β mRNA, thereby promoting glycolysis in HCC [52]. Whether MB targets G3BP1 to influence mitochondrial and lysosomal pathways remains to be further investigated. In this study, modulation of G3BP1 expression altered the expression of genes involved in N-glycosylation and affected ER stress. Given the central role of G3BP1 in SG assembly, we speculate that SGs mediate these effects under metabolic stress. SGs have been reported to interact with IRE1α during ER stress, influencing the IRE1α-XBP1 pathway [53]. In our study, reducing or inhibiting SG formation either through G3BP1 mutation or CHX inhibitor prevented the downregulation of N-glycosylation-related genes and alleviated ER stress. SGs induced by saturated fatty acids recruit PDX1 and disrupt its nucleocytoplasmic transport, thereby suppressing glucose-stimulated insulin secretion and contributing to pancreatic β-cell dysfunction [21]. Similarly, we observed that SGs recruit proteins associated with N-glycosylation, such as SEC61B and CANX, suppressing their interactions with partner proteins, and ultimately decreasing N-glycosylation efficiency. MB suppressed SG formation and subsequently blocked the recruitment of these proteins. This mechanism explains how MB restores N-glycosylation and alleviates ER stress.

## 5. Conclusion

In summary, MB significantly ameliorates the progression of MASH by enhancing N-glycosylation and ER stress. Mechanistically, MB inhibits G3BP1-mediated SG formation, thereby blocking the recruitment of key N-glycosylation-related proteins, including CANX and SEC61. Furthermore, MB suppresses SG assembly by inhibiting HDAC6-mediated deacetylation of G3BP1 under metabolic stress. Taken together, this study identifies G3BP1-dependent SG formation as a critical regulator of ER homeostasis in MASH and highlights MB as a promising therapeutic candidate that targets this pathway.

## Funding

This work was supported by the National Key R&D Program of China (No. 2023YFD1601400), Jiangsu Outstanding Youth Fund Project (No. BK20231535), National Natural Science Foundation of China (Nos. 82300685, 82430118), the Open Project of State Key Laboratory of Natural Medicines (SKLNMKF202501, SKLNMZZ2024JS25), Natural Science Foundation of Jiangsu Province (BK20221052), and the Basic Research Project for the Development of Modern Industrial College of Traditional Chinese Medicine and Health at Lishui University.

## Declaration of Competing Interests

These authors have no conflict of interest to declare.

## References

1 Ha S, Wong VWS, Zhang X, et al. Interplay between gut microbiome, host genetic and epigenetic modifications in MASLD and MASLD-related hepatocellular carcinoma. *Gut*. 2025;74(1):141-152. https://doi.org/10.1136/gutjnl-2024-332398.
2 Do A, Zahrawi F, Mehal WZ. Therapeutic landscape of metabolic dysfunction-associated steatohepatitis (MASH). *Nat Rev Drug Discov*. 2025;24(3):171-189. https://doi.org/10.1038/s41573-024-01084-2.
3 Younossi ZM, Stepanova M, Ong J, et al. Nonalcoholic steatohepatitis is the most rapidly increasing indication for liver transplantation in the United States. *Clin Gastroenterol Hepatol*. 2021;19(3):580-589. https://doi.org/10.1016/j.cgh.2020.05.064.
4 Gutiérrez-Cuevas J, Santos A, Armendariz-Borunda J. Pathophysiological molecular mechanisms of obesity: a link between MAFLD and NASH with cardiovascular diseases. *Int J Mol Sci*. 2021;22(21):11629. https://doi.org/10.3390/ijms222111629.
5 Quek J, Chan KE, Wong ZY, et al. Global prevalence of non-alcoholic fatty liver disease and non-alcoholic steatohepatitis in the overweight and obese population: a systematic review and meta-analysis. *Lancet Gastroenterol Hepatol*. 2023;8(1):20-30. https://doi.org/10.1016/S2468-1253(22)00317-X.
6 Lebeaupin C, Vallée D, Hazari Y, et al. Endoplasmic reticulum stress signalling and the pathogenesis of non-alcoholic fatty liver disease. *J Hepatol*. 2018;69(4):927-947. https://doi.org/10.1016/j.jhep.2018.06.008.
7 Baiceanu A, Mesdom P, Lagouge M, et al. Endoplasmic reticulum proteostasis in hepatic steatosis. *Nat Rev Endocrinol*. 2016;12(12):710-722. https://doi.org/10.1038/nrendo.2016.124.
8 Ajoolabady A, Kaplowitz N, Lebeaupin C, et al. Endoplasmic reticulum stress in liver diseases. *Hepatology*. 2023;77(2):619-639. https://doi.org/10.1002/hep.32562.
9 Harada Y, Ohkawa Y, Maeda K, et al. Glycan quality control in and out of the endoplasmic reticulum of mammalian cells. *FEBS J*. 2022;289(22):7147-7162. https://doi.org/10.1111/febs.16185.
10 Clarke JD, Novak P, Lake AD, et al. Impaired N-linked glycosylation of uptake and efflux transporters in human non-alcoholic fatty liver disease. *Liver Int*. 2017;37(7):1074-1081. https://doi.org/10.1111/liv.13362.
11 Chung CY, Majewska NI, Wang Q, et al. SnapShot: N-glycosylation processing pathways across kingdoms. *Cell*. 2017;171(1):258-258.e1. https://doi.org/10.1016/j.cell.2017.09.014.
12 Ramírez AS, Kowal J, Locher KP. Cryo-electron microscopy structures of human oligosaccharyltransferase complexes OST-A and OST-B. *Science*. 2019;366(6471):1372-1375. https://doi.org/10.1126/science.aaz3505.
13 Ruiz-Canada C, Kelleher DJ, Gilmore R. Cotranslational and posttranslational N-glycosylation of polypeptides by distinct mammalian OST isoforms. *Cell*. 2009;136(2):272-283. https://doi.org/10.1016/j.cell.2008.11.047.
14 Cavalcanti GV, de Oliveira FR, Bannitz RF, et al. Endoplasmic reticulum stress in the salivary glands of patients with primary and associated Sjögren's disease, and non-Sjögren's sicca syndrome: a comparative analysis and the influence of chloroquine. *Adv Rheumatol*. 2025;65(2):1-11. https://doi.org/10.1186/s42358-024-00430-7.
15 Chang J, Yang Q, Liu X, et al. Dihydroartemisinin inhibits ATP6 activity, reduces energy metabolism of hepatocellular carcinoma cells, promotes apoptosis and inhibits metastasis *via* CANX. *Oncol Lett*. 2024;28(4):474. https://doi.org/10.3892/ol.2024.14607.
16 Walter P, Ron D. The unfolded protein response: from stress pathway to homeostatic regulation. *Science*. 2011;334(6059):1081-1086. https://doi.org/10.1126/science.1209038.
17 Wang C, Cui Q, Du R, et al. Expression of G3BP1 in benign and malignant human prostate tissues. *Transl Androl Urol*. 2021;10(4):1665-1675. https://doi.org/10.21037/tau-20-1450.
18 Ge Y, Jin J, Li J, et al. The roles of G3BP1 in human diseases. *Gene*. 2022;821:146294. https://doi.org/10.1016/j.gene.2022.146294.
19 Aulas A, Caron G, Gkogkas CG, et al. G3BP1 promotes stress-induced RNA granule interactions to preserve polyadenylated mRNA. *J Cell Biol*. 2015;209(1):73-84. https://doi.org/10.1083/jcb.201408092.
20 Yang P, Mathieu C, Kolaitis RM, et al. G3BP1 is a tunable switch that triggers phase separation to assemble stress granules. *Cell*. 2020;181(2):325-345. https://doi.org/10.1016/j.cell.2020.03.046.
21 Zhang M, Yang C, Zhu M, et al. Saturated fatty acids entrap PDX1 in stress granules and impede islet beta cell function. *Diabetologia*. 2021;64(5):1144-1157. https://doi.org/10.1007/s00125-021-05389-4.
22 Amen T, Kaganovich D. Stress granules inhibit fatty acid oxidation by modulating mitochondrial permeability. *Cell Rep*. 2021;35(11):109237. https://doi.org/10.1016/j.celrep.2021.109237.
23 Lin L, Dong Y, Yang B, et al. Chemical constituents and biological activity of Chinese medicinal herb 'Xihuangcao'. *Comb Chem High Throughput Screen*. 2011;14(8):720-729. https://doi.org/10.2174/138620711796504352.
24 Li S, Liang F, Huang D, et al. Diterpenoids from the aerial parts of *Isodon serra* with selective cytotoxic activity. *Molecules*. 2024;29(12):2733. https://doi.org/10.3390/molecules29122733.
25 Liu X, Bian Z, Tian Y, et al. Six new diterpenoids with anti-inflammatory and cytotoxic activity from *Isodon serra*. *Fitoterapia*. 2024;176:106019. https://

doi.org/10.1016/j.fitote.2024.106019.
26 Zhang J, Yan J, Dong H, et al. Dimeric sesquiterpenoids with anti-inflammatory activities from *Inula britannica*. *Chin J Nat Med*. 2025;23(8):961-971. https://doi.org/10.1016/S1875-5364(25)60931-9.
27 Zhou H, Han M, Nan M, et al. Isodons AH, seco-abietane and abietane-type diterpenoids from *Isodon lophanthoides*: isolation, structural elucidation, and anticholestatic activity. *Chin J Nat Med*. 2025;23(9):1133-1142. https://doi.org/10.1016/S1875-5364(25)60977-0.
28 Lin CZ, Zhao W, Feng XL, et al. Cytotoxic diterpenoids from *Rabdosia lophanthoides* var. *gerardianus*. *Fitoterapia*. 2016;109:14-19. https://doi.org/10.1016/j.fitote.2015.11.015.
29 Feng F, Zhang W, Cao Y, et al. Combining label-free quantitative proteomics and 2D-DIGE to identify the potential targets of Sini decoction acting on myocardial infarction. *Chin J Nat Med*. 2025;23(8):1016-1024. https://doi.org/10.1016/S1875-5364(25)60937-X.
30 Li S, Xu F, Yu L, et al. Stigmasterol protects human brain microvessel endothelial cells against ischemia-reperfusion injury through suppressing EPHA2 phosphorylation. *Chin J Nat Med*. 2023;21(2):127-135. https://doi.org/10.1016/S1875-5364(23)60390-5.
31 Dolicka D, Foti M, Sobolewski C. The emerging role of stress granules in hepatocellular carcinoma. *Int J Mol Sci*. 2021;22(17):9428. https://doi.org/10.3390/ijms22179428.
32 Guay KP, Ke H, Canniff NP, et al. ER chaperones use a protein folding and quality control glyco-code. *Mol Cell*. 2023;83(24):4524-4537.e5. https://doi.org/10.1016/j.molcel.2023.11.006.
33 Fang MY, Markmiller S, Vu AQ, et al. Small-molecule modulation of TDP-43 recruitment to stress granules prevents persistent TDP-43 accumulation in ALS/FTD. *Neuron*. 2019;103(5):802-819. https://doi.org/10.1016/j.neuron.2019.05.048.
34 Cui Q, Bi H, Lv Z, et al. Diverse CMT2 neuropathies are linked to aberrant G3BP interactions in stress granules. *Cell*. 2023;186(4):803-820. https://doi.org/10.1016/j.cell.2022.12.046.
35 Markmiller S, Soltanieh S, Server KL, et al. Context-dependent and disease-specific diversity in protein interactions within stress granules. *Cell*. 2018;172(3):590-604. https://doi.org/10.1016/j.cell.2017.12.032.
36 Shrimal S, Cherepanova NA, Gilmore R. DC2 and KCP2 mediate the interaction between the oligosaccharyltransferase and the ER translocon. *J Cell Biol*. 2017;216(11):3625-3638. https://doi.org/10.1083/jcb.201702159.
37 Zhang J, Wang B, Gao X, et al. RNF185 regulates proteostasis in Ebolavirus infection by crosstalk between the calnexin cycle, ERAD, and reticulophagy. *Nat Commun*. 2022;13(1):6007. https://doi.org/10.1038/s41467-022-33805-9.
38 Xie Z, Zhao S, Tu Y, et al. Proteasome resides in and dismantles plant heat stress granules constitutively. *Mol Cell*. 2024;84(17):3320-3335. https://doi.org/10.1016/j.molcel.2024.07.033.
39 Anderson P, Kedersha N. RNA granules: post-transcriptional and epigenetic modulators of gene expression. *Nat Rev Mol Cell Biol*. 2009;10(6):430-436. https://doi.org/10.1038/nrm2694.
40 Gal J, Chen J, Na DY, et al. The acetylation of lysine-376 of G3BP1 regulates RNA binding and stress granule dynamics. *Mol Cell Biol*. 2019;39(22):e00052-19. https://doi.org/10.1128/MCB.00052-19.
41 Luo Z, Yin F, Wang X, et al. Progress in approved drugs from natural product resources. *Chin J Nat Med*. 2024;22(3):195-211. https://doi.org/10.1016/S1875-5364(24)60582-0.
42 Liu L, Liu Y, Zhang S, et al. Celastrol promotes apoptosis of breast cancer MDA-MB-231 cells by targeting HSDL2. *Acupunct Herb Med*. 2024;4(1):92-101. https://doi.org/10.1097/HM9.0000000000000102.
43 Sun CP, Zhou JJ, Yu ZL, et al. Kurarinone alleviated Parkinson's disease *via* stabilization of epoxyeicosatrienoic acids in animal model. *Proc Natl Acad Sci USA*. 2022;119(9):e2118818119. https://doi.org/10.1073/pnas.2118818119.
44 Zhang J, Luan ZL, Huo XK, et al. Direct targeting of sEH with alisol B alleviated the apoptosis, inflammation, and oxidative stress in cisplatin-induced acute kidney injury. *Int J Biol Sci*. 2023;19(1):294-310. https://doi.org/10.7150/ijbs.78097.
45 Feng YL, Xu XR, Zhu QM, et al. *Aucklandiae* radix targeted PKM2 to alleviate ulcerative colitis: insights from the photocrosslinking target fishing technique. *Phytomedicine*. 2024;134:155973. https://doi.org/10.1016/j.phymed.2024.155973
46 Zhang CH, Wang JX, Cai ML, et al. The roles and mechanisms of G3BP1 in tumour promotion. *J Drug Target*. 2019;27(3):300-305. https://doi.org/10.1080/1061186X.2018.1523415.
47 Omer A, Barrera MC, Moran JL, et al. G3BP1 controls the senescence-associated secretome and its impact on cancer progression. *Nat Commun*. 2020;11(1):4979. https://doi.org/10.1038/s41467-020-18734-9.
48 Wang Y, Fu D, Chen Y, et al. G3BP1 promotes tumor progression and metastasis through IL-6/G3BP1/STAT3 signaling axis in renal cell carcinomas. *Cell Death Dis*. 2018;9(5):501. https://doi.org/10.1038/s41419-018-0504-2.
49 Cherepanova N, Shrimal S, Gilmore R. N-linked glycosylation and homeostasis of the endoplasmic reticulum. *Curr Opin Cell Biol*. 2016;41:57-65. https://doi.org/10.1016/j.ceb.2016.03.021.
50 Ochoa-Rios S, O'Connor IP, Kent LN, et al. Imaging mass spectrometry reveals alterations in N-linked glycosylation that are associated with histopathological changes in nonalcoholic steatohepatitis in mouse and human. *Mol Cell Proteomics*. 2022;21(5):100225. https://doi.org/10.1016/j.mcpro.2022.100225.
51 Prentzell MT, Rehbein U, Sandoval MC, et al. G3BPs tether the TSC complex to lysosomes and suppress mTORC1 signaling. *Cell*. 2021;184(3):655-674.e27. https://doi.org/10.1016/j.cell.2020.12.024.
52 Ortega ÁD, Willers IM, Sala S, et al. Human G3BP1 interacts with β-F1-ATPase mRNA and inhibits its translation. *J Cell Sci*. 2010;123(16):2685-2696. https://doi.org/10.1242/jcs.065920.
53 Liu S, Zhang X, Yao X, et al. Mammalian IRE1α dynamically and functionally coalesces with stress granules. *Nat Cell Biol*. 2024;26(6):917-931. https://doi.org/10.1038/s41556-024-01418-7.